ADVANCED MATERIALS

www.advmat.de

Amide-Catalyzed Phase-Selective Crystallization Reduces Defect Density in Wide-Bandgap Perovskites

Junghwan Kim, Makhsud I. Saidaminov, Hairen Tan, Yicheng Zhao, Younghoon Kim, Jongmin Choi, Jea Woong Jo, James Fan, Rafael Quintero-Bermudez, Zhenyu Yang, Li Na Quan, Mingyang Wei, Oleksandr Voznyy, and Edward H. Sargent**

Wide-bandgap (WBG) formamidinium–cesium (FA-Cs) lead iodide–bromide mixed perovskites are promising materials for front cells well-matched with crystalline silicon to form tandem solar cells. They offer avenues to augment the performance of widely deployed commercial solar cells. However, phase instability, high open-circuit voltage (V_{oc}) deficit, and large hysteresis limit this otherwise promising technology. Here, by controlling the crystallization of FA-Cs WBG perovskite with the aid of a formamide cosolvent, light-induced phase segregation and hysteresis in perovskite solar cells are suppressed. The highly polar solvent additive formamide induces direct formation of the black perovskite phase, bypassing the yellow phases, thereby reducing the density of defects in films. As a result, the optimized WBG perovskite solar cells (PSCs) ($E_g \approx 1.75$ eV) exhibit a high V_{oc} of 1.23 V, reduced hysteresis, and a power conversion efficiency (PCE) of 17.8%. A PCE of 15.2% on 1.1 cm^2 solar cells, the highest among the reported efficiencies for large-area PSCs having this bandgap is also demonstrated. These perovskites show excellent phase stability and thermal stability, as well as long-term air stability. They maintain ≈95% of their initial PCE after 1300 h of storage in dry air without encapsulation.

Since the pioneering reports of lead halide perovskite solar cells (PSCs) in 2009, these materials have enabled a promising class of next-generation photovoltaic (PV) devices.[1–9] The power conversion efficiency (PCE) of solution-processed single-junction PSCs has recently achieved a certified record value of 22.1%, approaching comparability with that of single-junction crystalline silicon (c-Si) solar cells.[10] Another attractive application of PSCs is in a tandem architecture, in which the perovskites are integrated with mature Si-based PV. Tandem solar cells provide a means to overcome the Shockley–Queisser efficiency limit, offering a further path to reduce the cost per watt of solar electricity.[11–15]

Dr. J. Kim, Dr. M. I. Saidaminov, Dr. H. Tan, Y. Zhao, Dr. Y. Kim, Dr. J. Choi, Dr. J. W. Jo, J. Fan, R. Quintero-Bermudez, Dr. Z. Yang, Dr. L. N. Quan, M. Wei, Dr. O. Voznyy, Prof. E. H. Sargent
Department of Electrical and Computer Engineering
University of Toronto
10 King's College Road, Toronto, Ontario M5S 3G4, Canada
E-mail: o.voznyy@utoronto.ca; ted.sargent@utoronto.ca

DOI: 10.1002/adma.201706275

Wide-bandgap (WBG) perovskites with a bandgap of ≈1.75 eV as front cells are required in order to maximize the PCE of tandems with Si ($E_g \approx 1.1$ eV) back cells.[12,13] WBG perovskites can be synthesized by increasing the bromide (Br) content above 30% in any of the methylammonium-based ($MAPb(Br_xI_{1-x})_3$), formamidinium-based ($FAPb(Br_xI_{1-x})_3$), and their mixtures.[16–18] However, these suffer from phase segregation under illumination due to halide migration – Hoke's effect – leading to a high open-circuit voltage (V_{oc}) deficit (>500 meV) and poor photostability.[19–22]

Recently, innovative approaches to stabilizing WBG perovskites have been demonstrated, including increasing perovskite grain size;[23] and partially substituting MA/FA with Cs;[24,25] or Pb with Sn.[26] Among these next-generation perovskites, the composition $FA_{0.83}Cs_{0.17}Pb(I_{0.6}Br_{0.4})_3$ (hereafter, FA-Cs) shows improved phase stability and performance.[13,27] However, the V_{oc} of FA-Cs-based PSCs is still limited to <1.2 V, corresponding to a high deficit of 550 mV compared to ≈400 mV in lower-bandgap perovskite counterparts. In addition, long-term phase stability under full sunlight (AM 1.5G, 100 mW cm^{-2}) and hysteresis-free behavior remain to be demonstrated for this composition.

A key challenge in working with FA-Cs-based WBG perovskites resides in their high content of Cs and Br, whose salts poorly dissolve in conventional solvents.[28] Precipitated Cs and Br salts incorporate into ultimate films as undesired nonperovskite phases and induce defects.[29,30] These defects are detrimental to long-term phase stability, facilitate charge recombination losses, and induce hysteretic behavior. Incorporation of strong acids (57% w/w hydroiodic acid (HI) and 48% w/w hydrobromic acid (HBr) in water) into the precursor solution was proposed in recent reports;[13,26] however, in view of the known detrimental effect of water on the stability and hysteresis of PSCs,[31,32] we reasoned that pursuing a new strategy to reduce the defect densities would contribute to the realization of efficient and stable WBG PSCs.

Here, we enhance the V_{oc} and the stability of FA-Cs-based WBG perovskites by controlling film crystallization.

We introduce a highly polar additive, formamide (CH_3NO), into the precursor solution to increase the solubilization of the Cs salt, and we enable direct crystallization of the desired black phase, bypassing formation of the undesired yellow phase. Suppressing the formation of yellow δ-phases reduces the density of defects in the perovskite films. As a result, the WBG PSCs exhibit a PCE of 17.8% (a stabilized PCE of 17.2%) with a high V_{oc} of 1.23 V and low hysteresis. We also demonstrate a PCE of 15.2% on large area cells (1.1 cm^2). The improved WBG perovskites show excellent long-term phase-, thermal-, and air-stability: they maintain ≈95% of their initial PCE even after 1300 h storage in air without encapsulation.

We first studied the crystallization of FA-Cs WBG thin films fabricated using a previously reported method: spin-coating of perovskite solution in dimethylformamide (DMF) with the acid-water additives (57% w/w HI and 48% w/w HBr)[13] to aid in dissolving the Cs salts. We found that the as-deposited films contain nonperovskite phases such as H_2O–$FAPbI_3$ complex, yellow δ_O-$CsPbI_3$ and δ_H-$FAPbI_3$ (Figure S1, Supporting Information). Although these phases ultimately transform to perovskite after long annealing, this indirect pathway promotes the formation of defects.[33] We sought therefore a way to suppress the formation of undesired phases.

We took the view that a high-dielectric-constant amide additive could select in favor of forming the black perovskite phase. It promotes the dissolution of Cs salts and eliminates the necessity for the addition of water or strong acids. Formamide is a promising candidate since it dissolves Cs salts well[34] due to its high dielectric constant (ε = 109.5) compared to those of dimethyl sulfoxide (DMSO) (ε = 46.7) and DMF (ε = 37).

Control films (c-FA-Cs) show dramatic differences from films prepared with formamide additive (f-FA-Cs) (**Figure 1**). Detailed information for the film preparation is provided in the Experimental Section and Table S1 (Supporting Information). The as-deposited c-FA-Cs films display orange color (Figure 1a(i)) and contains nonperovskite phases (Figure 1b(i)), including FAI–PbI_2–DMSO complex (2θ = 7.0°), PbI_2–DMSO adduct (2θ = 9.2°, 18.5°), yellow δ_H-$FAPbI_3$ (2θ = 11.8°), yellow δ_H-$FAPb(I_{0.6}Br_{0.4})_3$ (2θ = 12.5°), and CsI (2θ = 27.8°).[6,27] After annealing, the film turns dark and forms the perovskite phase (Figure 1b(ii)).

In contrast to c-FA-Cs, the as-deposited f-FA-Cs displays the pure perovskite phase (Figure 1a(iii)) (X-ray diffraction (XRD), Figure 1b(iii), (iv)). Fourier-transform infrared spectroscopy (FT-IR) revealed enhanced perovskite crystallization aided by formamide (Figure 1c). The f-FA-Cs film exhibited a strong stretching vibration peaks of C=N (at 1714 cm^{-1}) and of N−H (at 3270 and 3408 cm^{-1}) from FA^+: this indicates enhanced crystallinity of the f-FA-Cs even without thermal annealing.[35] The lack of the C=O stretching peak at 1662 cm^{-1}, a fingerprint of formamide, points to its catalytic role: it promotes crystallization without being incorporated into final perovskite films (Figure S2, Supporting Information).

We also studied the effect of the formamide on the composition and morphology of films by X-ray photoelectron spectroscopy (XPS) and scanning electron microscopy (SEM). The content of Cs and Br in f-FA-Cs was increased by 40% and 17%, respectively, compared to those in c-FA-Cs (**Figure 2**a–c and Table S2 (Supporting Information)) due to the increased solubility of the Cs salt and crystallization dynamics. Figure S3 and Table S2 (Supporting Information) summarize the XPS data for Cs, Pb, I, Br and their content. Also, the f-FA-Cs films showed smoother and more compact surfaces compared to that of the c-FA-Cs (Figure 2d,e and Figures S4 and S5 (Supporting Information)).

To explore the effect of formamide-assisted crystallization on the carrier recombination dynamics of perovskite films, we measured the time-resolved photoluminescence (PL) traces (Figure 2f). By fitting the data with a biexponential function (Figure 2f), we found that f-FA-Cs exhibits longer bulk carrier lifetime (τ_2) of 385 ns, surpassing $\tau_2 \approx$ 235 ns of c-FA-Cs. The threefold enhancement of steady-state PL intensity and the weaker dependence of V_{oc} on the light intensity in f-FA-Cs films indicate reduced trap-assisted nonradiative recombination via formamide-assisted crystallization of perovskites (Figures S6 and S7, Supporting Information).[36–38]

Next, we investigated the effect of formamide modification on the light-induced phase stability under an intensity of 100 mW cm^{-2}. FA-MA-Cs-based WBG perovskite ($FA_{0.81}MA_{0.14}Cs_{0.05}PbBr_{1.2}I_{1.8}$)[39] served as an additional control. Figure S8a–c (Supporting Information) presents the PL spectra of FA-MA-Cs, f-FA-Cs, and c-FA-Cs WBG perovskites after continuous illumination with AM 1.5G with an intensity of 100 mW cm^{-2} for 60 min. For the FA-MA-Cs WBG perovskite, the initial PL peak at ≈700 nm continuously shifts to longer wavelengths (lower energy) with illumination time. This is also accompanied by a broadening of the PL bandwidth. These are due to the phase segregation of the film (Figure S8a, Supporting Information). In contrast, both the FA-Cs WBG perovskites show excellent phase stability with negligible PL peak shift (Figure S8b,c, Supporting Information). Although their full width at half maximum (FWHM) values broadened slightly (≈10 nm), they were saturated after a few minutes of illumination and maintained their shapes after 60 min illumination. Notably, the f-FA-Cs film showed two times slower FWHM broadening compared to c-FA-Cs.

We also investigated the thermal stability of the WBG perovskites. We kept films at 100 °C in N_2 atmosphere and measured their absorption spectra for 60 h (Figure S9a–c, Supporting Information). The absorption of the FA-MA-Cs perovskite after 60 h thermal stress decreased by 50%, indicating significant degradation of the perovskite phase. We attribute the phase instability of FA-MA-Cs to the presence of volatile MA (14%), which readily decomposes into CH_3NH_2 and HI (or HBr) and sublimes.[31] However, the c-FA-Cs maintained 70% of their initial film absorption (Figure S9d, Supporting Information). The f-FA-Cs WBG perovskites showed the highest thermal resistance, exhibiting 85% of their initial film absorption after 60 h thermal stress. Thus, the f-FA-Cs WBG perovskites with higher content of Cs exhibit enhanced thermal and phase stability. This is consistent with our observation of fewer impurities in the films, suggesting a reduced amount of defect sites associated with the increased Cs and Br contents.[20,22,40]

To quantify the effect of formamide-assisted crystallization on the performance of PSCs, we fabricated solar cells in indium tin oxide (ITO)/Cl-TiO_2/perovskite/spiro/Au architecture.[9] The

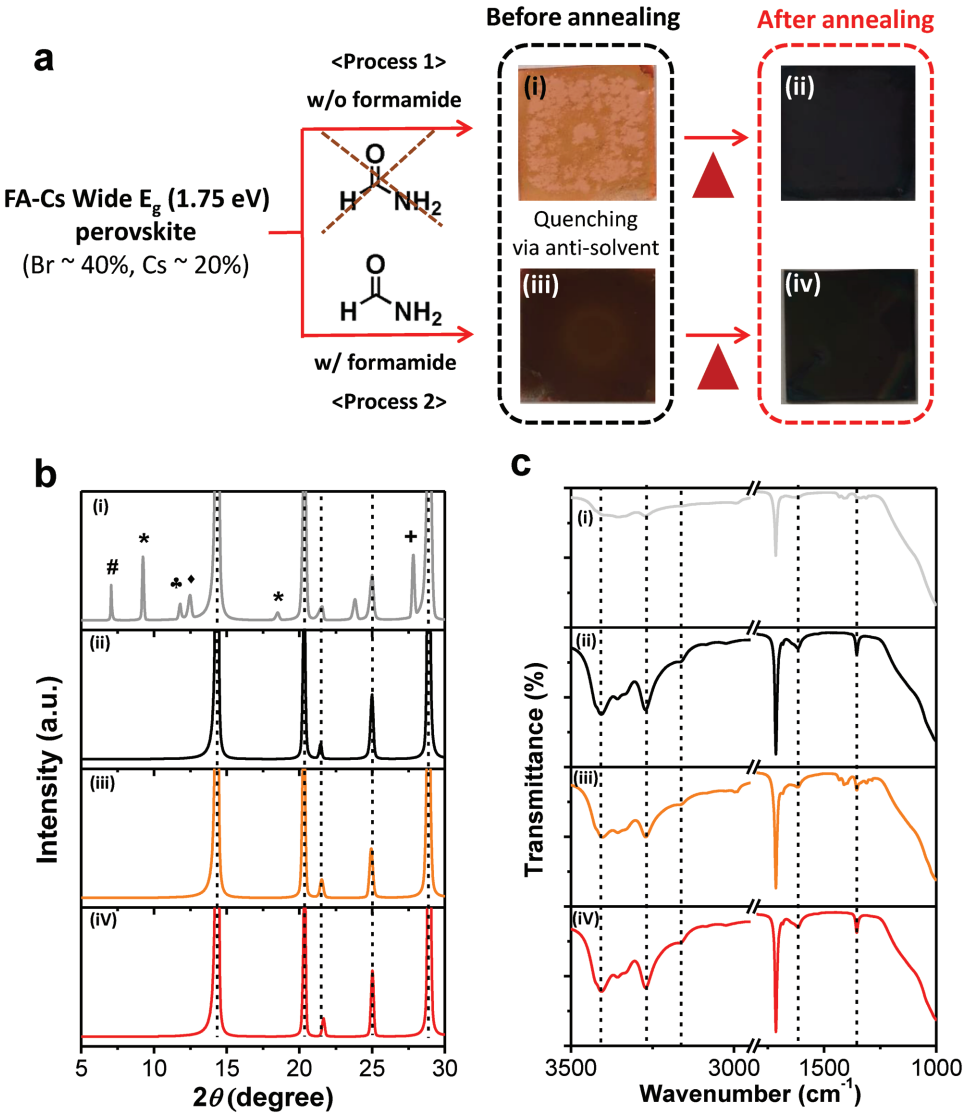

Figure 1. Crystallization of FA-Cs WBG perovskites. a) FA-Cs WBG perovskite formation process without and with formamide additive. The chemical structure of formamide is also shown. (i) The as-deposited film without formamide, (ii) the annealed perovskite film without formamide, (iii) the as-deposited film with formamide, and (iv) the annealed perovskite film with formamide. b) XRD and c) FT-IR spectra of the (i), (ii), (iii), and (iv) films. The dashed lines indicate crystalline peaks and organic cations of perovskites, respectively. For the XRD spectrum of film (i), peaks of #, *, ◆, ♣, and + represent FAI–PbI_2–DMSO complex, PbI_2–DMSO complex, δ_H-$FAPbI_3$, δ_H-$FAPb(I_{0.6}Br_{0.4})_3$, and CsI, respectively.

photovoltaic parameters of these devices are summarized in Figure S10 and Table S3 (Supporting Information). PSCs based on the c-FA-Cs film exhibited a PCE of 16.6% (a stabilized PCE ≈ 16.0%) with a short-circuit current density (J_{sc}) of 18.11 mA cm^{-2}, a V_{oc} of 1.20 V, and a fill factor (FF) of 76%, comparable to those of the reported FA-Cs-based WBG PSCs[13] (**Figure 3**a). PSCs based on f-FA-Cs showed remarkably improved performance: a PCE of 17.8% (a stabilized PCE ≈ 17.2%), J_{sc} of 18.34 mA cm^{-2}, V_{oc} of 1.23 V, and a FF of 79% (Figure S11, Supporting Information). The J_{sc} value is well matched with the external quantum efficiency measurement (Figure S12, Supporting Information). We also fabricated large-area (1.1 cm^2) PSCs based on f-FA-Cs and demonstrated a PCE of 15.2% (Figure 3b), the highest performance among the reported large-area WBG perovskites with E_g ≈ 1.75 eV.

We also tested the long-term stability of PSCs (Figure 3c). The unencapsulated PSCs were stored in the dark in dry air and their PCEs were measured over time. The f-FA-Cs-based PSCs maintained ≈95% of their initial PCEs even after 1300 h storage. In contrast, the c-FA-Cs WBG PSC lost 60% of the initial PCE within less than 1000 h.

We now turn to the hysteresis behavior of FA-Cs WBG perovskites. PSCs with c-FA-Cs showed a strong hysteretic behavior (Figure S13, Supporting Information) that is comparable to previously published values for materials having similar composition.[41] In contrast, PSCs based on f-FA-Cs showed substantially reduced hysteresis. Since the hysteretic behavior is affected by space charges trapped at the interface between the perovskite and the carrier-transporting layers, we treated the surface of f-FA-Cs WBG perovskites with methylammonium iodide (MAI) solution

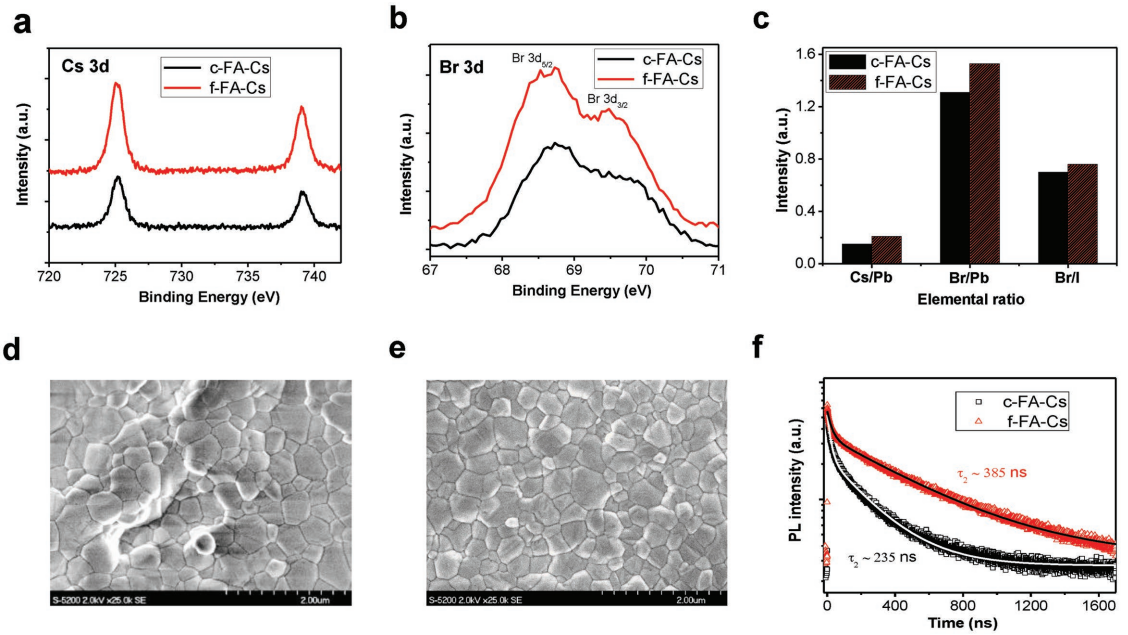

Figure 2. Characterization of films. a,b) The core-level XPS spectra of Cs 3d and Br 3d of the perovskite films without (c-FA-Cs) and with (f-FA-Cs) formamide additive. c) The atomic ratio of Cs/Pb, Br/Pb, and Br/I. d,e) SEM images and f) time-resolved PL decay of the c-FA-Cs and f-FA-Cs films.

(0.25 wt% in isopropyl alcohol (IPA)) to suppress the hysteresis further. The MAI-treated f-FA-Cs devices showed negligible hysteresis, and retained the PCE. This finding agrees with the recent studies[39,42] and suggests that the hysteresis of the FA-Cs WBG PSCs can be addressed by optimizing the interface between the perovskite and the hole transport layer/electron transport layer. We do note, however, that the MAI-treated f-FA-Cs PSCs degraded faster due to rapid MA evaporation, which has been seen to occur in MA-based perovskites. The best performance and stability were obtained using the f-FA-Cs WBG perovskites without MA. This finding indicates that a novel-and-stable interface modifier will, when developed and deployed, help to address the challenge of hysteresis without compromise to stability, an important subject for future studies.

In conclusion, we investigated the effect of crystallization dynamics on defect formation, light-induced phase segregation, thermal stability, and device performance of the FA-Cs-based WBG perovskites. The highly polar solvent additive of formamide enabled direct formation of perovskites and suppressed the formation of nonperovskite phases. As a result, the f-FA-Cs WBG perovskites showed excellent light-induced phase-, thermal-, and air-stability, as well as device performance with a high V_{oc} of 1.23 V. The hysteresis of the FA-Cs-based WBG PSCs was remarkably suppressed by the synergistic effect of formamide. These findings highlight the importance of direct perovskite crystallization and the high solubilizing ability for the Cs salt for efficient and stable WBG perovskites with high Cs and Br contents. This study paves the way for developing stable and performing WBG perovskites that are sought for efficient perovskite/c-Si tandem devices.

Experimental Section

Chemicals and Reagents: PbI_2 beads (99.999%), $PbBr_2$ powder (99.999%), CsI powder (99.9%), and anhydrous solvents were purchased from Sigma-Aldrich. FAI and MABr were purchased from Dyesol Limited (Australia). All salts and solvents were used as received without any further purification.

Preparation of Solution—FA-Cs WBG Perovskites: FAI, CsI, PbI_2, and $PbBr_2$ were dissolved in 0.9 mL of DMSO:DMF (2:7 v/v ratio) mixture solution in the following molar ratios to get a composition of 1.2 M $FA_{0.83}Cs_{0.17}Pb(I_{0.6}Br_{0.4})_3$:$PbI_2$/$PbBr_2$ = 0.4:0.6, FAI/CsI = 0.83:0.17, and (FAI + CsI)/(PbI_2 + $PbBr_2$) = 1:1. After stirring at 40 °C for 3 h on a hot plate in N_2, 100 µL of the stock solutions (DMSO:formamide = 9:1, 7:3, 5:5 v/v ratio) was added to the 1.2 M perovskite precursor solution to get 1, 3, and 5 vol% formamide-added precursors, respectively. The best performance was obtained from the 3 vol% addition (see Table S1 in the Supporting Information). Therefore, all film characterizations were carried out at that concentration. For control precursor solution, 100 µL of the DMSO solvent was added to the 1.2 M precursor solution. It was found that the solubility of mixed salts is poor in pure formamide. The best recipe for preparation of FA-Cs WBG perovskites was achieved by using a synergetic effect of the mixed cosolvents (DMF:DMSO:formamide). The FA-Cs WBG perovskites with 57% w/w HI and 48% w/w HBr additives were introduced by following the previous works.[13,26]

Preparation of Solution—FA-MA-Cs WBG Perovskite: FAI, CsI, MABr, PbI_2, $PbBr_2$ were dissolved in DMSO:DMF (1:4) mixture solution in the following molar ratios: PbI_2/$PbBr_2$ = 0.5:0.5, CsI/FAI/MABr = 0.05:0.81:0.14, and (FAI + MABr + CsI)/(PbI_2 + $PbBr_2$) = 1:1 to get the final concentration of 1.4 M.

Preparation of Solution—Spiro Solution: Spiro solution was prepared by dissolving 67.5 mg of spiro-2,2′,7,7′-tetrakis-(*N*,*N*-di-p-methoxyphenylamine)-9,9′-spirobifluorene (spiro-OMeTAD) in 1 mL chlorobenzene with addition of 25 µL of *tert*-butylpyridine, as well as 35 µL of bis(trifluoromethane)sulfonimide lithium salt (300 mg mL^{-1} in acetonitrile).

Perovskite Solar Cell Fabrication: The prepatterned ITO (TFD Devices)-coated glasses were cleaned by acetone and isopropanol. After drying the ITO substrates, the Cl-capped TiO_2 was spin-coated on the ITO substrates, and annealed on a hot plate at 150 °C for 30 min in ambient air. The preparation method of the Cl-capped TiO_2 solution is reported elsewhere.[9] The perovskite films were deposited onto the TiO_2 substrates with the two-step spin-coating procedures. For the FA-Cs WBG perovskites, the first step was 1000 rpm for 10 s with an

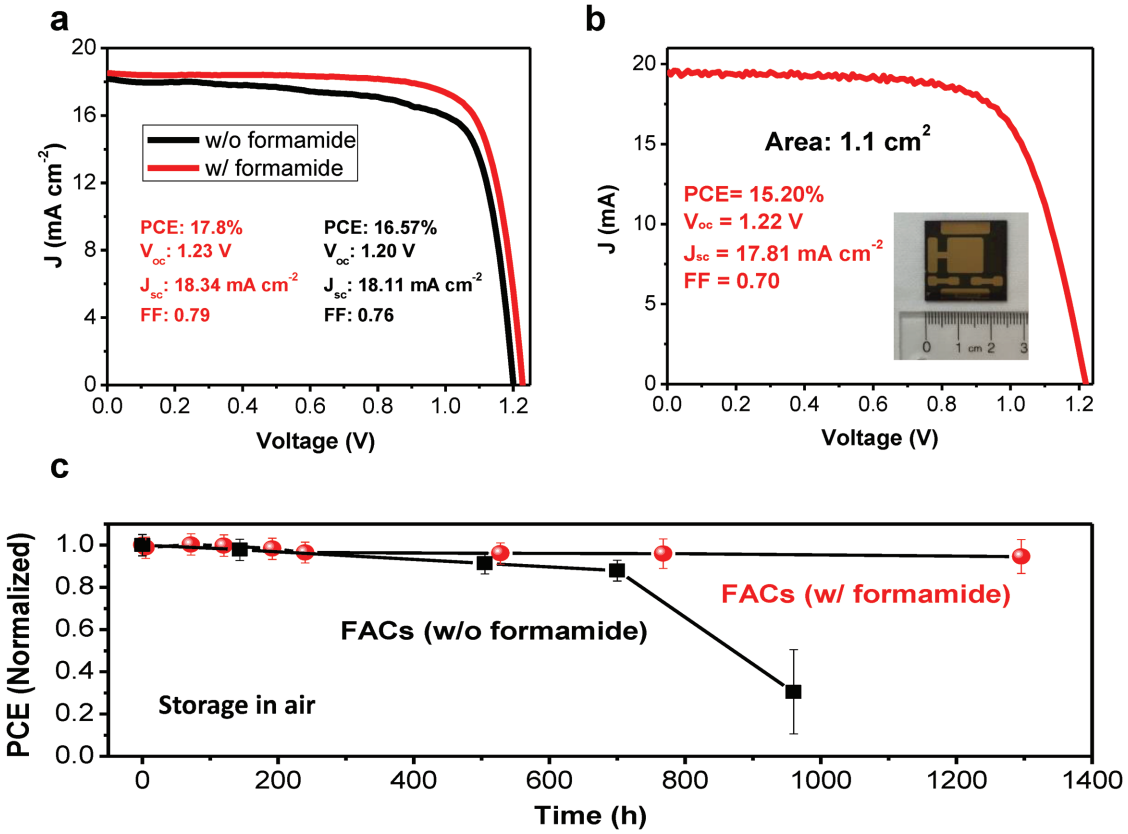

Figure 3. Performance and stability of FA-Cs-based WBG PSCs. a) *J–V* characteristics of the FA-Cs WBG PSCs (area of 4.9 mm^2) incorporating FA-Cs without and with formamide additive. b) *J–V* characteristic curve of the best large-area FA-Cs device with an active area of 1.1 cm^2. c) Dark storage stability of the unencapsulated PSCs using FA-Cs (without and with formamide). The devices were kept in the dry box (<30% relative humidity) in the dark and measured regularly in nitrogen.

acceleration of 250 rpm s^{-1} and the second step was 2000 rpm for 60 s with a ramp-up of 2000 rpm s^{-1}. Chlorobenzene (500 µL) was dropped on the spinning substrate during the second spin-coating step at 35 s before the end of the procedure. The substrates were then immediately transferred on a hotplate and heated at 100 °C for 30 s and then at 160 °C for 10 min. To further reduce the hysteresis, the f-FA-Cs film was treated with MAI solution (0.25 wt% in IPA) by spin-casting at 5000 rpm for 30 s, and annealing at 100 °C for 5 min. In the case of the FA-MA-Cs WBG perovskites, the first step was 1000 rpm for 10 s with an acceleration of 250 rpm s^{-1}. Spin speed of 6000 rpm for 20 s with a ramp-up of 2000 rpm s^{-1} was followed for the second step and 300 µL chlorobenzene was dropped on the spinning substrates during the second spin-coating step at 5 s before the end of the procedure. The substrate was then immediately transferred on a hot plate and heated at 100 °C for 20 min. Then, the spiro solution was deposited by spin-coating at 4000 rpm for 30 s. Finally, the 100 nm Au contact was deposited on top of spiro-OMeTAD by electron-beam evaporation.

Solar Cell Characterization: The *J–V* characteristics were measured using a Keithley 2400 sourcemeter under the illumination of the solar simulator (Newport, Class A) at the light intensity of 100 mW cm^{-2} in N_2 atmosphere (Sciencetech class A). Unless otherwise stated, the *J–V* curves were measured with a scanning rate of 500 mV s^{-1} (voltage step of 10 mV and delay time of 20 ms). An aperture shade mask with area of 4.9 mm^2 and 1 cm^{-2} was placed in front of the small- and large-area solar devices, respectively, to avoid overestimation of the photocurrent density. The dark long-term stability assessment of solar cells was carried out by repeating the *J–V* characterizations after storage in the dark with various times. The devices without encapsulation were stored in a cabinet with ambient air with relative humidity < 30%.

Other Characterizations: XRD patterns were collected using a Rigaku MiniFlex 600 diffractometer equipped with a NaI scintillation counter and using monochromatized Copper Kα radiation (λ = 1.5406 Å). XPS analysis was carried out using the Thermo Scientific K-Alpha XPS system, with a 300 µm spot size, 75 eV pass energy, and energy steps of 0.05 eV. Optical absorption measurements were carried out in a Lambda 950 UV/Vis spectrophotometer. The Thermo Scientific Nicolet iS50 attenuated total reflectance (ATR)-FT-IR was used to obtain the FT-IR spectra. Spectra were obtained using 8 scans with a resolution of 2 cm^{-1}, and the collection range was between 550 and 4000 cm^{-1}. PL was measured using a Horiba Fluorolog time correlated single-photon-counting system with photomultiplier tube detectors. The excitation source is a laser diode at a wavelength of 504 nm and the detector has collected PL signals at 710 nm.

Supporting Information

Supporting Information is available from the Wiley Online Library or from the author.

Acknowledgements

J.K. and M.I.S. contributed equally to this work. This publication was based partly on the work supported by the Ontario Research Fund Research Excellence Program, and by the Natural Sciences and Engineering Research Council of Canada. M.I.S. acknowledges

the support from the Banting Postdoctoral Fellowship program, administered by the Natural Sciences and Engineering Research Council (NSERC) of Canada. H.T. acknowledges The Netherlands Organization for Scientific Research (NWO) for a Rubicon grant (680-50-1511) in support of his postdoctoral research at the University of Toronto. This work was made possible by the NPRP grant # 8-086-1-017 from the Qatar National Research Fund (a member of Qatar Foundation). The findings achieved herein were solely the responsibility of the authors. The authors thank R. Wolowiec, D. Kopilovic, L. Levina, and E. Palmiano for their help during the course of study.

Conflict of Interest

The authors declare no conflict of interest.

Keywords

amides, defects, perovskite solar cells, wide-bandgap perovskites

Received: October 29, 2017
Revised: December 8, 2017
Published online:

[1] A. Kojima, K. Teshima, Y. Shirai, T. Miyasaka, *J. Am. Chem. Soc.* **2009**, *131*, 6050.
[2] H.-S. Kim, C.-R. Lee, J.-H. Im, K.-B. Lee, T. Moehl, A. Marchioro, S.-J. Moon, R. Humphry-Baker, J.-H. Yum, J. E. Moser, M. Grätzel, N.-G. Park, *Sci. Rep.* **2012**, *2*, 591.
[3] M. M. Lee, J. Teuscher, T. Miyasaka, T. N. Murakami, H. J. Snaith, *Science* **2012**, *338*, 643.
[4] J. Burschka, N. Pellet, S.-J. Moon, R. Humphry-Baker, P. Gao, M. K. Nazeeruddin, M. Gratzel, *Nature* **2013**, *499*, 316.
[5] N. J. Jeon, J. H. Noh, Y. C. Kim, W. S. Yang, S. Ryu, S. Il Seok, *Nat. Mater.* **2014**, *13*, 897.
[6] N. J. Jeon, J. H. Noh, W. S. Yang, Y. C. Kim, S. Ryu, J. Seo, S. Il Seok, *Nature* **2015**, *517*, 476.
[7] N. Ahn, D. Y. Son, I. H. Jang, S. M. Kang, M. Choi, N. G. Park, *J. Am. Chem. Soc.* **2015**, *137*, 8696.
[8] M. Saliba, T. Matsui, J.-Y. Seo, K. Domanski, J.-P. Correa-Baena, M. K. Nazeeruddin, S. M. Zakeeruddin, W. Tress, A. Abate, A. Hagfeldt, M. Grätzel, *Energy Environ. Sci.* **2016**, *9*, 1989.
[9] H. Tan, A. Jain, O. Voznyy, X. Lan, F. P. García de Arquer, J. Z. Fan, R. Quintero-Bermudez, M. Yuan, B. Zhang, Y. Zhao, F. Fan, P. Li, L. N. Quan, Y. Zhao, Z.-H. Lu, Z. Yang, S. Hoogland, E. H. Sargent, *Science* **2017**, *355*, 722.
[10] W. S. Yang, B.-W. Park, E. H. Jung, N. J. Jeon, Y. C. Kim, D. U. Lee, S. S. Shin, J. Seo, E. K. Kim, J. H. Noh, S. Il Seok, *Science* **2017**, *356*, 1376.
[11] K. A. Bush, A. F. Palmstrom, Z. J. Yu, M. Boccard, R. Cheacharoen, J. P. Mailoa, D. P. McMeekin, R. L. Z. Hoye, C. D. Bailie, T. Leijtens, I. M. Peters, M. C. Minichetti, N. Rolston, R. Prasanna, S. Sofia, D. Harwood, W. Ma, F. Moghadam, H. J. Snaith, T. Buonassisi, Z. C. Holman, S. F. Bent, M. D. McGehee, *Nat. Energy* **2017**, *2*, 17009.
[12] Z. Yu, M. Leilaeioun, Z. Holman, *Nat. Energy* **2016**, *1*, 16137.
[13] D. P. McMeekin, G. Sadoughi, W. Rehman, G. E. Eperon, M. Saliba, M. T. Horantner, A. Haghighirad, N. Sakai, L. Korte, B. Rech, M. B. Johnston, L. M. Herz, H. J. Snaith, *Science* **2016**, *351*, 151.
[14] C. D. Bailie, M. G. Christoforo, J. P. Mailoa, A. R. Bowring, E. L. Unger, W. H. Nguyen, J. Burschka, N. Pellet, J. Z. Lee, M. Grätzel, R. Noufi, T. Buonassisi, A. Salleo, M. D. McGehee, *Energy Environ. Sci.* **2015**, *8*, 956.
[15] S. Albrecht, M. Saliba, J. P. Correa Baena, F. Lang, L. Kegelmann, M. Mews, L. Steier, A. Abate, J. Rappich, L. Korte, R. Schlatmann, M. K. Nazeeruddin, A. Hagfeldt, M. Grätzel, B. Rech, *Energy Environ. Sci.* **2016**, *9*, 81.
[16] J. H. Noh, S. H. Im, J. H. Heo, T. N. Mandal, S. Il Seok, *Nano Lett.* **2013**, *13*, 1764.
[17] G. E. Eperon, S. D. Stranks, C. Menelaou, M. B. Johnston, L. M. Herz, H. J. Snaith, *Energy Environ. Sci.* **2014**, *7*, 982.
[18] C. Bi, Y. Yuan, Y. Fang, J. Huang, *Adv. Energy Mater.* **2015**, *5*, 1.
[19] E. T. Hoke, D. J. Slotcavage, E. R. Dohner, A. R. Bowring, H. I. Karunadasa, M. D. McGehee, *Chem. Sci.* **2015**, *6*, 613.
[20] D. J. Slotcavage, H. I. Karunadasa, M. D. McGehee, *ACS Energy Lett.* **2016**, *1*, 1199.
[21] S. J. Yoon, S. Draguta, J. S. Manser, O. Sharia, W. F. Schneider, M. Kuno, P. V. Kamat, *ACS Energy Lett.* **2016**, *1*, 290.
[22] A. J. Barker, A. Sadhanala, F. Deschler, M. Gandini, S. P. Senanayak, P. M. Pearce, E. Mosconi, A. J. Pearson, Y. Wu, A. R. Srimath Kandada, T. Leijtens, F. De Angelis, S. E. Dutton, A. Petrozza, R. H. Friend, *ACS Energy Lett.* **2017**, *2*, 1416.
[23] Y. Chen, M. He, J. Peng, Y. Sun, Z. Liang, *Adv. Sci.* **2016**, *3*, 1500392.
[24] C. Yi, J. Luo, S. Meloni, A. Boziki, N. Ashari-Astani, C. Grätzel, S. M. Zakeeruddin, U. Röthlisberger, M. Grätzel, *Energy Environ. Sci.* **2016**, *9*, 656.
[25] J. W. Lee, D. H. Kim, H. S. Kim, S. W. Seo, S. M. Cho, N. G. Park, *Adv. Energy Mater.* **2015**, *5*, 1501310.
[26] Z. Yang, A. Rajagopal, S. B. Jo, C. C. Chueh, S. Williams, C. C. Huang, J. K. Katahara, H. W. Hillhouse, A. K. Y. Jen, *Nano Lett.* **2016**, *16*, 7739.
[27] W. Rehman, D. P. McMeekin, J. B. Patel, R. L. Milot, M. B. Johnston, H. J. Snaith, L. M. Herz, *Energy Environ. Sci.* **2017**, *10*, 361.
[28] R. E. Beal, D. J. Slotcavage, T. Leijtens, A. R. Bowring, R. A. Belisle, W. H. Nguyen, G. F. Burkhard, E. T. Hoke, M. D. McGehee, *J. Phys. Chem. Lett.* **2016**, *7*, 746.
[29] G. E. Eperon, G. M. Paternò, R. J. Sutton, A. Zampetti, A. A. Haghighirad, F. Cacialli, H. J. Snaith, *J. Mater. Chem. A* **2015**, *3*, 19688.
[30] Y. Yu, C. Wang, C. R. Grice, N. Shrestha, J. Chen, D. Zhao, W. Liao, A. J. Cimaroli, P. J. Roland, R. J. Ellingson, Y. Yan, *ChemSusChem* **2016**, *9*, 3288.
[31] T. Leijtens, K. Bush, R. Cheacharoen, R. Beal, A. Bowring, M. D. McGehee, *J. Mater. Chem. A* **2017**, *5*, 11483.
[32] C. Clegg, I. G. Hill, *RSC Adv.* **2016**, *6*, 52448.
[33] M. Saliba, T. Matsui, K. Domanski, J.-Y. Seo, A. Ummadisingu, S. M. Zakeeruddin, J.-P. Correa-Baena, W. R. Tress, A. Abate, A. Hagfeldt, M. Gratzel, *Science* **2016**, *354*, 206.
[34] D. Zhao, S. Li, Q. Zhai, Y. Jiang, M. Hu, *J. Chem. Thermodyn.* **2014**, *78*, 134.
[35] Z. Zhou, S. Pang, F. Ji, B. Zhang, G. Cui, *Chem. Commun.* **2016**, *52*, 3828.
[36] J. Kim, G. Kim, T. K. Kim, S. Kwon, H. Back, J. Lee, S. H. Lee, H. Kang, K. Lee, *J. Mater. Chem. A* **2014**, *2*, 17291.
[37] S. R. Cowan, A. Roy, A. J. Heeger, *Phys. Rev. B* **2010**, *82*, 245207.
[38] A. K. K. Kyaw, D. H. Wang, V. Gupta, J. Zhang, S. Chand, G. C. Bazan, A. J. Heeger, *Adv. Mater.* **2013**, *25*, 2397.
[39] Y. Lin, B. Chen, F. Zhao, X. Zheng, Y. Deng, Y. Shao, Y. Fang, Y. Bai, C. Wang, J. Huang, *Adv. Mater.* **2017**, *29*, 1.
[40] M. Hu, C. Bi, Y. Yuan, Y. Bai, J. Huang, *Adv. Sci.* **2015**, *3*, 6.
[41] Y. Yu, C. Wang, C. R. Grice, N. Shrestha, D. Zhao, W. Liao, L. Guan, R. A. Awni, W. Meng, A. J. Cimaroli, K. Zhu, R. J. Ellingson, Y. Yan, *ACS Energy Lett.* **2017**, *2*, 1177.
[42] Q. Jiang, L. Zhang, H. Wang, X. Yang, J. Meng, H. Liu, Z. Yin, J. Wu, X. Zhang, J. You, *Nat. Energy* **2016**, *1*, 16177.